Energy Efficient Full-Range Oscillation Analysis of Parallel-Plate Electrostatically Actuated MEMS Resonators *

Andreu Fargas-Marquès & Ramon Costa-Castelló
Universitat Politècnica de Catalunya (UPC)

Abstract

Electrostatic parallel-plate actuators are a common way of actuating microelectromechanical systems, both statically and dynamically. Nevertheless, actuation voltages and oscillations are limited by the nonlinearity of the actuator that leads to the *Pull-in* phenomena. This work presents a new approach to obtain the electrostatic parallel-plate actuation voltage, which allows to freely select the desired frequency and amplitude of oscillation. Harmonic Balance analysis is used to determine the needed actuation voltage and to choose the most energy efficient actuation frequency. Moreover, a new two-sided actuation approach is presented that allows to actuate the device in all the stable range using the *Harmonic Balance Voltage*.

1 Introduction

Microelectromechanical systems (MEMS) based on the electrostatic parallel-plate actuation principle are seemingly simple to fabricate and operate (Fig. 1). For this reason, they are the basic building block for a wide variety of sensors. The list include accelerometers [31] and gyroscopes [21], temperature sensors [10], gas sensors [4] and mass sensors [28] among others. The main challenge is the nonlinearity of the parallel-plate electrostatic force that leads to the *Pull-in* phenomena [8].

Several techniques, such as mechanical modifications [17], voltage patterns [7, 23] or different electrode configurations [18] have been considered to increase the stable static and dynamic range of actuation of parallel-plate electrostatic actuators. However, they focus on avoiding the *Pull-in* problem and, in that effort, they limit the actuation amplitude and oscillation frequency.

*This work has been supported by the projects DPI2015-69286-C3-2-R of the Spanish Ministerio de Educación de España MINECO/FEDER and 2014 SGR 267 of the AGAUR agency of the Generalitat de Catalunya.

The use of different frequencies in the actuation of MEMS resonators, and their effect on the stability and sensor bandwidth has been widely analyzed in the case of parametric excitation [9, 19, 22]. Lately, new approaches have focused on the effect of secondary resonance [3], multiple modes of oscillation and different frequencies [13, 14, 15, 33], or multiple harmonics [20].

Research has shown the beneficial effects of multiple harmonics on the stability and performance of MEMS resonators. Applying different frequencies to excite multiple modes of oscillation is shown in [16] to produce large bandwidth in the resonator response. At the same time, the fact of using the combination of two different frequency sources allows to tune the bandwidth of the resonator as desired.

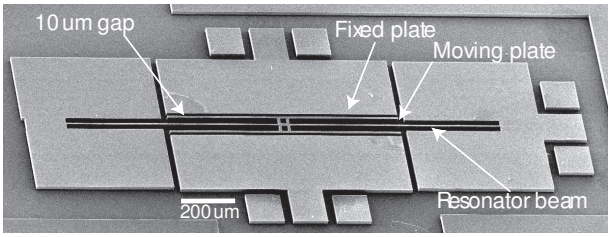

Figure 1: An example of a fabricated beam resonator with parallel-plate electrostatic actuation and sensing. The parameters of this design have been used for simulations [8].

This paper analyzes the capability of multiple harmonic actuation in order to improve oscillation performance, while avoiding the pull-in phenomena in steady state. For the first time, a constructive analytical voltage harmonic content selection algorithm is derived to freely select the oscillation amplitude and frequency of the MEMS device.

Moreover, the presented analysis takes into account energy storage, transfer and power dissipation in oscillatory steady-state response of electrostatically actuated MEMS structures to finally select the most energy efficient frequency of oscillation.

This analysis leads to the definition of a new two-sided actuation configuration that allows to actuate a parallel-plate electrostatically actuated MEMS device at any desired oscillation amplitude and frequency in the stable oscillation range.

In Section 2, the nonlinear model of the MEMS system is presented and a concentrated parameters simplification is derived to apply Harmonic Balance. In Section 3, Harmonic Balance is applied to derive the equilibrium equations in steady-state oscillation. In Section 4, the Harmonic Balance Voltage is presented and its capabilities and complexity analyzed. In Section 5, the Harmonic Balance Voltage energy consumption is analyzed to be able to determine minimum energy frequencies. In Section 6, a new two sided actuation approach is presented to be able to use Harmonic Balance Voltage to freely choose the amplitude and frequency of oscillation in all the stable range of oscillations. And

in Section 7, final conclusions and future work are presented.

2 Nonlinear actuator MEMS model

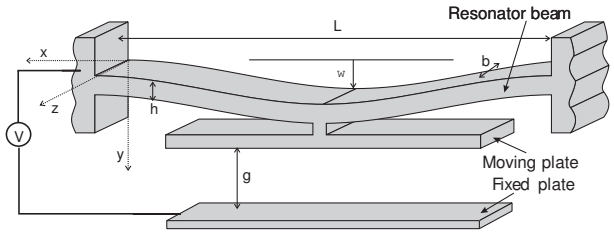

Figure 2: Basic scheme of a deflected beam with electrostatic parallel-plate actuation, which is a schematic representation of most MEMS devices. Using the Galerkin Method [24], the deformation of a beam is studied as the lumped mass-spring-damper system in Fig. 3.

Figure 2 shows a schematic beam representation of a parallel-plate electrostatically actuated MEMS resonator. Most MEMS resonators can be assimilated to this representation.

Using differential equations to derive mechanical deformations, electrostatic forces and the damping forces, the dynamics of the system can be reduced to [1]:

$$\rho \mathrm{A}\frac{\partial^2 \hat{w}}{\partial t^2} + c_d\frac{\partial \hat{w}}{\partial t} + \mathrm{E'I}\frac{\partial^4 \hat{w}}{\partial \hat{x}^4} - \left[\hat{N}(t) + \frac{\mathrm{E'A}}{2\mathrm{L}}\int_0^{\mathrm{L}}\left(\frac{\partial \hat{w}}{\partial \hat{x}}\right)^2 \mathrm{d}\hat{x}\right]\frac{\partial^2 \hat{w}}{\partial \hat{x}^2} = \hat{F}_{elec}(t) \quad (1)$$

given the following boundary conditions

$$\hat{w}(0,t) = \hat{w}(\mathrm{L},t) = 0, \quad \hat{w}'(0,t) = \hat{w}'(\mathrm{L},t) = 0,$$

where $\hat{w}(\hat{x},t)$ is the oscillation amplitude at position $\hat{x}$ and time t, $\hat{N}(t)$ is any axial force applied to the beam, $\hat{F}_{elec}(t)$ is the applied electrostatic force, c_d is the calculated damping constant of the system, ρ is the density of the beam, A is the area of the cross-section of the beam ($\mathrm{A} = \mathrm{b}\cdot\mathrm{h}$, b and h are the width and height of the section of the beam), L is the longitude of the beam, I is the moment of inertia of the cross-section ($\mathrm{I} = \mathrm{bh}^3/12$), and $\mathrm{E'} = \mathrm{E}/(1-\nu^2)$ where E is the Young Modulus and ν is the Poisson ratio.

The Galerkin Method [24] can be used to convert the partial differential equation, (1), into a single-degree of freedom ordinary differential equation. This allows to deal with a mass-spring-damper concentrated parameter model (Fig. 3) with a voltage-controlled actuation. This approach is the most popular in the literature [5, 6, 12, 25, 26].

Firstly, the beam response is assumed to be composed of an infinite number of oscillation modes, and consequently, the displacement $\hat{w}$ can be decomposed in

$$\hat{w}(\hat{x},t) = \sum_{i=0}^{\infty} \hat{q}_i(t)\hat{\phi}_i(\hat{x}) \tag{2}$$

where $\hat{q}_i(t)$ is the time-dependent modal displacement for the oscillation mode i and $\hat{\phi}_i(\hat{x})$ is the position-dependent modal shape.

Equation (2) can be substituted in the previously presented equation (1) to obtain the dynamics equation for each vibration mode of the beam [24]

$$M_{eff,i} \cdot \ddot{\hat{q}}_i + B_{eff,i} \cdot \dot{\hat{q}}_i + K_{eff,i} \cdot \hat{q}_i + K_{3,eff,i} \cdot \hat{q}_i^3 = F_{eff,i} \tag{3}$$

where the effective mechanical constants for each mode of oscillation are derived as

$$M_{eff,i} = \rho \mathrm{A} \int_0^{\mathrm{L}} \hat{\phi}_i^2 \mathrm{d}\hat{x} \tag{4}$$

$$K_{eff,i} = \mathrm{EI} \int_0^{\mathrm{L}} \left(\frac{\partial^2 \hat{\phi}_i}{\partial \hat{x}^2} \right)^2 \mathrm{d}\hat{x} + \hat{N}(\hat{t}) \int_0^{\mathrm{L}} \left(\frac{\partial \hat{\phi}_i}{\partial \hat{x}} \right)^2 \mathrm{d}\hat{x} \tag{5}$$

$$K_{3,eff,i} = \frac{\mathrm{EA}}{2\mathrm{L}} \left[\int_0^{\mathrm{L}} \left(\frac{\partial \hat{\phi}_i}{\partial \hat{x}} \right)^2 \mathrm{d}\hat{x} \right]^2 \tag{6}$$

$$B_{eff,i} = \hat{c}_d \int_0^{\mathrm{L}} \hat{\phi}_i^2 \mathrm{d}\hat{x}. \tag{7}$$

At the same time, the electrostatic force associated with the actuator capacitor is defined as

$$F_{eff_i} = \frac{1}{2} \frac{\mathrm{C}}{(1 - \frac{\hat{q}_i(t)}{\mathrm{g}_0})} V^2, \tag{8}$$

where $\mathrm{C} = \frac{\varepsilon_0 \mathrm{A}_c}{\mathrm{g}_0} \left(1 + 0.65 \frac{\mathrm{g}_0}{\mathrm{b}}\right)$ is the capacitance at rest using a first-order fringing field correction [11], ε_0 is the dielectric constant, g_0 is the initial gap between the plates, b is the device thickness, A_c is the area of the plates, and V is the applied voltage between the electrodes.

Assuming, as usual, that the system behavior is sufficiently captured by the first mode of oscillation, the dynamic response of the beam in Fig. 2 can be modeled by the lumped mass-spring-damper in Fig. 3, given that $\hat{q}_1(t) \simeq \hat{y}(t)$, $\mathrm{M}_{eff,1} \simeq \mathrm{M}$, $\mathrm{K}_{eff,1} \simeq \mathrm{K}$, $\mathrm{K}_{3,eff,i} \simeq \mathrm{K}_3$, $\mathrm{B}_{eff,1} \simeq \mathrm{B}$ and $\mathrm{F}_{eff,1} \simeq \mathrm{F}$. The consideration of higher order modes would improve the accuracy of the model, as shown in [32], but at expense of an increase in the mathematical complexity.

Consequently, the dynamics of the system can be described by

$$\mathrm{M}\ \ddot{\hat{y}} + \mathrm{B}\ \dot{\hat{y}} + \mathrm{K}\ \hat{y} + \mathrm{K}_3\ \hat{y}^3 = \frac{1}{2} \frac{\mathrm{C}_0}{\mathrm{g}_0 (1 - \frac{\hat{y}}{\mathrm{g}_0})^2} V^2. \tag{9}$$

This is the dynamic equation of a mass-spring-damper system with parallel-plate electrostatic actuation and a nonlinear spring (Fig. 3).

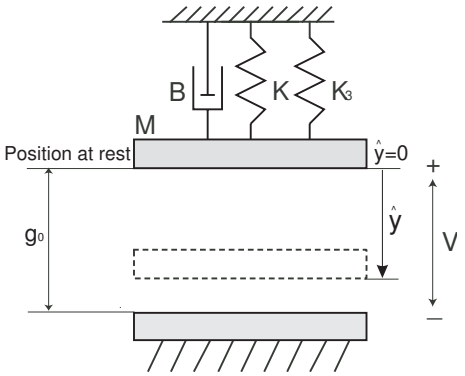

Figure 3: Schematics of an electromechanical system with parallel-plate actuation. It includes a linear spring, a nonlinear spring and linear velocity damping.

For the Harmonic Balance formulation, it is best to work with the resulting normalized actuation gap, $g = 1 - \hat{y}/\mathrm{g_0}$, and once substituted into (9), the resulting equation is

$$-\frac{d^2g}{dt^2} - \frac{\omega_\mathrm{n}}{\mathrm{Q}}\frac{dg}{dt} + \omega_\mathrm{n}^2(1-g) + \kappa(1-g)^3 = \mathrm{f}_k\mathrm{g}_k\frac{V^2}{g^2} \tag{10}$$

where $\mathrm{C_0} = \frac{\epsilon \mathrm{A_c}}{\mathrm{g_0}}$, $\mathrm{f}_k = \frac{\mathrm{C_0}}{2\mathrm{g_0}}$, $\mathrm{g}_k = \frac{1}{\mathrm{g_0 M}}$, $\frac{\mathrm{B}}{\mathrm{M}} = \frac{\omega_\mathrm{n}}{\mathrm{Q}}$, $\frac{\mathrm{K}}{\mathrm{M}} = \omega_\mathrm{n}^2$ and $\kappa = \frac{\mathrm{K_3 g_0^2}}{\mathrm{M}}$, being ω_n the natural frequency of the system, $\mathrm{Q} = \frac{1}{2\zeta}$ the quality factor and ζ the damping of the system.

Rearranging terms

$$\Big(-\big(\frac{d^2g}{dt^2} + \frac{\omega_\mathrm{n}}{\mathrm{Q}}\frac{dg}{dt} + \omega_\mathrm{n}^2 g + \kappa g^3\big) + \omega_\mathrm{n}^2 + \kappa - 3\kappa g + 3\kappa g^2\Big)g^2 = \mathrm{f}_k\mathrm{g}_k V^2 \tag{11}$$

and introducing

$$H(g) = \frac{d^2g}{dt^2} + \frac{\omega_\mathrm{n}}{\mathrm{Q}}\frac{dg}{dt} + \omega_\mathrm{n}^2 g + \kappa g^3 \tag{12}$$

the equation converts to

$$-H(g)g^2 + (\omega_\mathrm{n}^2 + \kappa)g^2 - 3\kappa g^3 + 3\kappa g^4 = \mathrm{f}_k\mathrm{g}_k V^2 \tag{13}$$

3 Harmonic Balance steady-state characterization

Equation (13) establishes the relationship between the position (gap distance $g(t)$) and the voltage (actuator driving voltage $V(t)$). If the system is analyzed in steady-state oscillation, both variables can be approximated using Fourier series.

The gap distance can be expressed, in steady state, as

$$g(t) = \sum_{n=-\infty}^{\infty} \breve{G}_n e^{j\,n\,\omega\,t} \tag{14}$$

where $\breve{G}_n \in \mathbb{C}$ is the amplitude of the n-th harmonic oscillation in exponential form.

From equation (14), the velocity and acceleration of the gap, in steady state, can be computed as

$$\frac{dg(t)}{dt} = \sum_{n=-\infty}^{\infty} jn\omega\breve{G}_n e^{jn\omega t}, \tag{15}$$

$$\frac{d^2g(t)}{dt^2} = \sum_{n=-\infty}^{\infty} -n^2\omega^2\breve{G}_n e^{jn\omega t}. \tag{16}$$

All the higher order terms of the position are expressed as follow

$$g(t)^2 = \sum_{n=-\infty}^{\infty} \alpha_n e^{jn\omega t} \text{ with } \alpha_n = \sum_{p=-\infty}^{\infty} \breve{G}_{n-p}\breve{G}_p, \tag{17}$$

$$g(t)^3 = \sum_{n=-\infty}^{\infty} \tau_n e^{jn\omega t} \text{ with } \tau_n = \sum_{r=-\infty}^{\infty} \breve{G}_{n-r}\alpha_r, \tag{18}$$

$$g(t)^4 = \sum_{n=-\infty}^{\infty} \delta_n e^{jn\omega t} \text{ with } \delta_n = \sum_{q=-\infty}^{\infty} \alpha_{n-q}\alpha_q. \tag{19}$$

And the $H(g)$ term, defined in (12), becomes

$$H(g) = \sum_{n=-\infty}^{\infty} \Lambda_n e^{jn\omega t}$$

where $\Lambda_n = (-\omega^2\,n^2 + j\,\frac{\omega_n}{Q}\,\omega\;n + \omega_n^2)\,\breve{G}_n + \kappa\tau_n$.

At the same time, the input voltage is assumed to be

$$V(t) = \sum_{n=-\infty}^{\infty} \breve{V}_n\, e^{j\,n\,\omega\,t} \tag{20}$$

where $\breve{V}_n$ is the n-th harmonic amplitude of the voltage. This implies that the square of the input is

$$V(t)^2 = \sum_{n=-\infty}^{\infty} \beta_n e^{jn\omega t} \text{ with } \beta_n = \sum_{p=-\infty}^{\infty} \breve{V}_{n-p}\breve{V}_p \tag{21}$$

being β_n the n-th order amplitude.

Using these definitions on equation (13) and rearranging terms, the complete system dynamics can be represented as follows

$$\sum_{n=-\infty}^{\infty}\Bigg(-\sum_{q=-\infty}^{\infty}\Lambda_q\,\alpha_{n-q} + (\omega_{\mathrm{n}}^2+\kappa)\alpha_n - 3\kappa\tau_n + 3\kappa\delta_n\Bigg)e^{jn\omega t} = \sum_{n=-\infty}^{\infty}\mathrm{f}_k\mathrm{g}_k\beta_n e^{jn\omega t} \tag{22}$$

Equation (22) generates the following set of equations to be solved for each harmonic:

$$\begin{aligned}
-\sum_{q=-\infty}^{\infty}\Lambda_q\alpha_{-q} + (\omega_{\mathrm{n}}^2+\kappa)\alpha_0 - 3\kappa\tau_0 + 3\kappa\delta_0 &= \mathrm{f}_k\mathrm{g}_k\beta_0\\
-\sum_{q=-\infty}^{\infty}\Lambda_q\alpha_{1-q} + (\omega_{\mathrm{n}}^2+\kappa)\alpha_1 - 3\kappa\tau_1 + 3\kappa\delta_1 &= \mathrm{f}_k\mathrm{g}_k\beta_1\\
-\sum_{q=-\infty}^{\infty}\Lambda_q\alpha_{-1-q} + (\omega_{\mathrm{n}}^2+\kappa)\alpha_{-1} - 3\kappa\tau_{-1} + 3\kappa\delta_{-1} &= \mathrm{f}_k\mathrm{g}_k\beta_{-1}\\
-\sum_{q=-\infty}^{\infty}\Lambda_q\alpha_{2-q} + (\omega_{\mathrm{n}}^2+\kappa)\alpha_2 - 3\kappa\tau_2 + 3\kappa\delta_2 &= \mathrm{f}_k\mathrm{g}_k\beta_2\\
-\sum_{q=-\infty}^{\infty}\Lambda_q\alpha_{-2-q} + (\omega_{\mathrm{n}}^2+\kappa)\alpha_{-2} - 3\kappa\tau_{-2} + 3\kappa\delta_{-2} &= \mathrm{f}_k\mathrm{g}_k\beta_{-2}\\
&\ldots \quad \text{for n}
\end{aligned}$$

These equations define the relationship between the gap oscillation and the input voltage in steady state. Consequently, given an input voltage the steady-state oscillation can be predicted. On the other way round, they can also be used to select the voltage needed for a desired steady-state oscillation. This voltage has been named as *Harmonic Balance Voltage* (HBV).

4 Harmonic Balance Voltage

4.1 Harmonic Balance Voltage definition

The introduction of the HBV allows to change the parallel-plate electrostatic actuation paradigm in MEMS resonators. The oscillation is not defined by the voltage, on the contrary, the voltage is fixed by the desired oscillation.

The HBV, $V_{\mathrm{HBV}}(t)$, is defined as

$$V_{\mathrm{HBV}}(t)^2 = \sum_{i=0}^{\infty} \beta_i \, e^{j\,i\,\omega\,t} + \sum_{i=1}^{\infty} \bar{\beta}_i \, e^{-j\,i\,\omega\,t} \tag{23}$$

where $\bar{\beta}_i$ is the complex conjugate of β_i and the β_i terms are calculated as follows:

$$\beta_i = \frac{1}{\mathrm{f_k g_k}} \Big(- \sum_{q=-\infty}^{\infty} \Lambda_q \, \alpha_{i-q} + (\omega_{\mathrm{n}}^2 + \kappa)\alpha_i - 3\kappa\tau_i + 3\kappa\delta_i \Big) \tag{24}$$

Consequently, the complexity of the HBV would depend on the desired oscillation and the system parameters. This complexity for most common approaches is summarized in Table 1. As can be observed, a minimum of four real-valued equations must be solved in order to obtain β_0 to β_3 for a perfect sinusoidal oscillation if the model does not contain a nonlinear mechanical spring. On the other side, if the oscillation has up to three harmonics and the model contains a nonlinear spring, the HBV is composed of β_0 up to β_{15}.

Case	Needed terms
Linear spring ($\kappa = 0$) - 1 harmonic	β_0 to β_3
Linear spring ($\kappa = 0$) - 2 harmonics	β_0 to β_6
Linear spring ($\kappa = 0$) - 3 harmonics	β_0 to β_9
Nonlinear spring ($\kappa \neq 0$) - 1 harmonic	β_0 to β_5
Nonlinear spring ($\kappa \neq 0$) - 2 harmonics	β_0 to β_{10}
Nonlinear spring ($\kappa \neq 0$) - 3 harmonics	β_0 to β_{15}

Table 1: Summary of usual system models and desired oscillation patterns, with their corresponding number of harmonics needed in the actuation voltage, based on HBV calculation.

4.2 Pure sinusoidal oscillation

In most practical device implementations, pure sinusoidal oscillation is desired. The HBV allows to calculate which is the appropriate actuation voltage that achieves the desired pure sinusoidal oscillation.

Assuming that the system evolution is a pure sinusoidal, the gap distance, g, reduces to

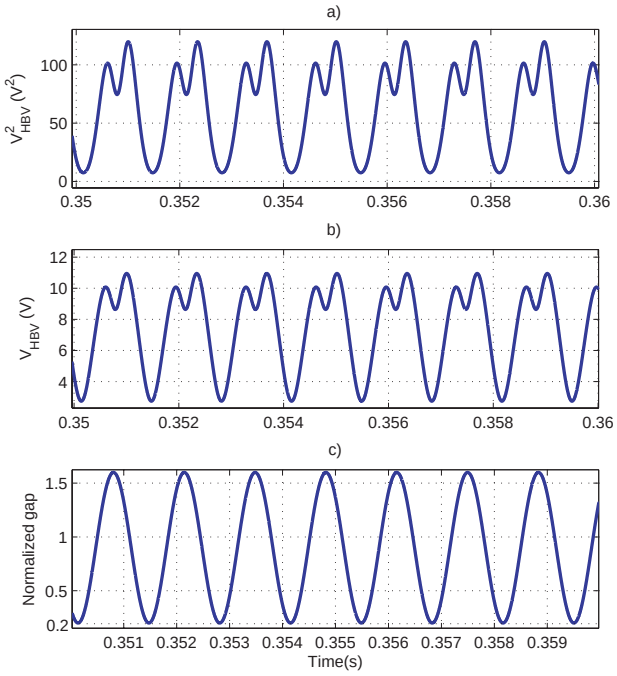

Figure 4: HBV calculation for an oscillation with damping Q = 100 and frequency of $0.96\omega_{\mathrm{n}}$, to obtain a static gap position of $G_0 = 0.9$ and an amplitude of oscillation of $G_1 = 0.7$. a) Calculated $V_{\mathrm{HBV}}(t)^2$ from β_i and Equation (23). b) HBV, $V_{\mathrm{HBV}}(t)$, as square-root of a). c) Simulated output of the system, where it can be observed that it satisfies the desired oscillation.

$$g(t) = G_0 + G_1 \sin(\omega t + \phi_1) = \breve{G}_0 + \breve{G}_1 e^{j\omega t} + \breve{G}_{-1} e^{-j\omega t}$$

where $\breve{G}_0 = G_0$, $\breve{G}_1 = \frac{G_1}{2j} e^{j\phi_1}$ and $\breve{G}_{-1} = \overline{\breve{G}_1}$ is the conjugate of $\breve{G}_1$.

Then, the actuation voltage is obtained using (23), and the β_i terms, assuming nonlinear mechanical spring are reduced to the following equations(24):

$$
\begin{aligned}
\beta_0 =& \frac{1}{\mathrm{f}_k \mathrm{g}_k}\Big[-\omega_\mathrm{n}^2\breve{G}_0^3+\omega_\mathrm{n}^2\breve{G}_0^2+\big(4\omega^2-6\omega_\mathrm{n}^2\big)|\breve{G}_1|^2\breve{G}_0+2\omega_\mathrm{n}^2|\breve{G}_1|^2\Big]\\
&+\frac{\kappa}{\mathrm{f}_k \mathrm{g}_k}\Big[-\breve{G}_0^5+3\breve{G}_0^4-3\breve{G}_0^3+\breve{G}_0^2-30|\breve{G}_1|^4\breve{G}_0-20|\breve{G}_1|^2\breve{G}_0^3\\
&+36|\breve{G}_1|^2\breve{G}_0^2+18|\breve{G}_1|^4-18|\breve{G}_1|^2\breve{G}_0+2|\breve{G}_1|^2\Big]\\
\beta_1 =& \frac{1}{\mathrm{f}_k \mathrm{g}_k}\Big[\big(3\omega^2-j\frac{\omega_\mathrm{n}}{\mathrm{Q}}\omega-3\omega_\mathrm{n}^2\big)|\breve{G}_1|^2\\
&+\big(\omega^2-j\frac{\omega_\mathrm{n}}{\mathrm{Q}}\omega-3\omega_\mathrm{n}^2\big)\breve{G}_0^2+2\omega_\mathrm{n}^2\breve{G}_0\Big]\breve{G}_1\\
&+\frac{\kappa}{\mathrm{f}_k \mathrm{g}_k}\Big[-10|\breve{G}_1|^4-30|\breve{G}_1|^2\breve{G}_0^2-5\breve{G}_0^4+36|\breve{G}_1|^2\breve{G}_0\\
&+12\breve{G}_0^3-9|\breve{G}_1|^2-9\breve{G}_0^2+2\breve{G}_0\Big]\breve{G}_1\\
\beta_2 =& \frac{1}{\mathrm{f}_k \mathrm{g}_k}\Big[\big(2\omega^2-2j\frac{\omega_\mathrm{n}}{\mathrm{Q}}\omega-3\omega_\mathrm{n}^2\big)\breve{G}_0+\omega_\mathrm{n}^2\Big]\breve{G}_1^2\\
&+\frac{\kappa}{\mathrm{f}_k \mathrm{g}_k}\Big[-20|\breve{G}_1|^2\breve{G}_0-10\breve{G}_0^3+12|\breve{G}_1|^2+18\breve{G}_0^2-9\breve{G}_0+1\Big]\breve{G}_1^2\\
\beta_3 =& \frac{1}{\mathrm{f}_k \mathrm{g}_k}\big[\omega^2-j\frac{\omega_\mathrm{n}}{\mathrm{Q}}\omega-\omega_\mathrm{n}^2\big]\breve{G}_1^3\\
&+\frac{\kappa}{\mathrm{f}_k \mathrm{g}_k}\big[-5|\breve{G}_1|^2-10\breve{G}_0^2+12\breve{G}_0-3\big]\breve{G}_1^3\\
\beta_4 =& \frac{\kappa}{\mathrm{f}_k \mathrm{g}_k}\big[-5\breve{G}_0+3\big]\breve{G}_1^4\\
\beta_5 =& -\frac{\kappa}{\mathrm{f}_k \mathrm{g}_k}\breve{G}_1^5
\end{aligned}
$$

where $|\breve{G}_n|$ is the absolute value of $\breve{G}_n$.

For a chosen oscillation amplitude, G_0 and G_1, these equations provide the required control action, $V_{\mathrm{HBV}}(t)$. An example of the calculated actuation voltage and the obtained oscillation is shown in Fig. 4. In the presented example, an static gap displacement of $G_0 = 0.9$ is desired, as well as, an amplitude of oscillation of $G_1 = 0.7$. These features are imposed for a frequency close to resonance, $0.96\omega_\mathrm{n}$, and medium damping conditions, $\mathrm{Q} = 100$. Equation (23) allows to determine the HBV, but squared, $V_{\mathrm{HBV}}(t)^2$, as shown in Fig. 4a. From this value, the actual HBV can be derived, $V_{\mathrm{HBV}}(t)$, by square-root of the previous value (Fig. 4b). This value, obtained using numerical fitting tools, can be used to generate a signal to drive the MEMS resonator. Fig. 4c shows the simulated oscillation of the MEMS resonator model used in the example (Table 2). As can be seen, the desired static displacement and oscillation amplitude are obtained.

4.3 Harmonic Balance Voltage complexity

The HBV allows to obtain the desired oscillation amplitude and frequency. However, that doesn't mean that it can be easily used to drive a real device. The

pattern can be complex, and must be converted to a number of voltage signals ready to be delivered in an actuation set-up.

A first problem arises from HBV analysis. Depending on the desired oscillation, the calculated actuation voltage from the β-equations cannot always be reproduced as the square of a sinusoidal signal. As can be seen in Fig. 5, the calculated voltage, $V_{\mathrm{HBV}}(t)^2$, takes negative values. This means that the signal cannot be generated by squaring the input voltage $V(t)$. This leads to the impossibility to reach the desired oscillation with a classical one-sided voltage driving scheme.

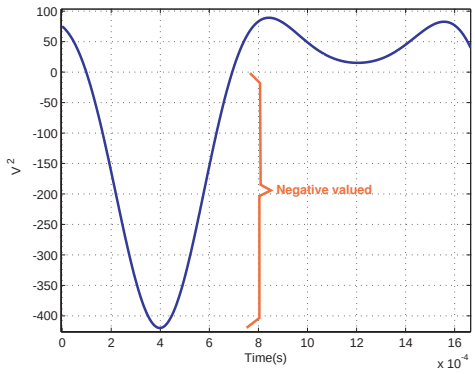

Figure 5: HBV calculation ($V_{\mathrm{HBV}}(t)^2$) for an oscillation with medium damping, $\mathrm{Q} = 100$, and low frequency, $0.8\omega_{\mathrm{n}}$. It is desired to obtain a static gap position of $G_0 = 0.9$ and an amplitude of oscillation of $G_1 = 0.7$. This voltage is directly obtained from the β_i of the Harmonic Balance equations. As can be observed, the signal has negative values.

Apart from that limitation, some calculated actuation voltages can also be difficult to reproduce. No closed-form expression is available to obtain the input voltage from $V_{\mathrm{HBV}}(t)^2$, when it has been calculated. Consequently, the final driving voltage, $V_{\mathrm{HBV}}(t)$, must be obtained by numerically solving the implicit equations. In that case, the input signal is assumed with a predefined number of harmonics, in order to solve the equations. In the example in Fig. 6, at least five harmonics are needed to produce a good numerical solution for the input voltage, while perfect reproduction is achieved with ten harmonics.

In order to analyze the complexity of the HBV in front of different system parameters, iterative solutions have been calculated. Presented examples are based on the device parameters from Table 2. At each step, HBV is approximated using an rsquare-error minimization technique to determine the minimum number of harmonics needed to obtain an *rsquare*-error of unity. The results are calculated on a square grid with 2 degrees of freedom: X-axis corresponds to the static displacement (G_0) ranging from 0.7 to 1 and the Y-axis corresponds to the oscillation amplitude (G_1) ranging from 0.05 to 0.9.

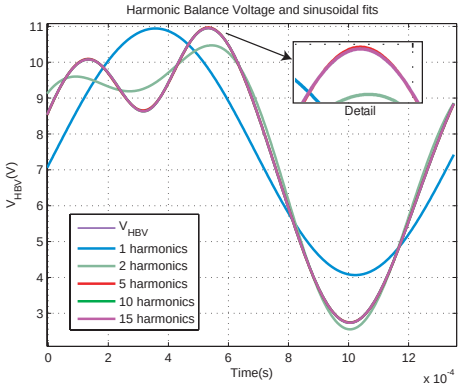

Figure 6: Sinusoidal implicit solution of the HBV for an oscillation with damping Q = 100, a frequency of $0.96\omega_{\mathrm{n}}$, a static gap position of $G_0 = 0.9$ and an amplitude of oscillation of $G_1 = 0.7$. The solutions obtained (1 to 15 Harmonics) for the input voltage are compared. In the figure, the 5, 10 and 15 harmonics solutions are almost overlapped with the calculated V_{HBV} curve. Consequently, the 5 harmonics solution is already close to the calculated V_{HBV}, and the 10 harmonics solution can be considered almost identical.

Fig. 7 shows the number of harmonics needed to reproduce an input voltage that obtain the desired oscillation given by the X(G_0)-Y(G_1) axis. The plots are obtained for three different frequencies ($0.9\omega_{\mathrm{n}}$, $0.96\omega_{\mathrm{n}}$, ω_{n}). The plots show the effect of selected frequency on the desired input voltage and the number of harmonics needed to reproduce it. Same tests have been carried on for different damping values, but they have small effect on the voltage pattern and complexity.

In the plots, the region on the right (*red zone*) indicates that the voltage solution calculated by the harmonic balance equations is not completely positive-valued, and consequently, the zone cannot be reached by one-sided voltage actuation (Fig. 5). The region on top (*brown zone*) is the area that cannot be achieved due to the fact that the total amplitude is greater than the physical gap. The orange areas indicate that with 10 harmonics the calculated input voltage is not satisfactorily generated.

The plots analysis shows that with frequencies closer to natural frequency (between $0.96\,\omega_{\mathrm{n}}$ and ω_{n}), it is easier to obtain a pure sinusoidal oscillation: the range of obtainable oscillations is wider, and large amplitudes can be achieved with few harmonics in the input. When the desired frequencies are further away ($0.9\,\omega_{\mathrm{n}}$ and below), the range of achievable oscillations diminishes and the difficulty to calculate the input voltage increases, as observed by the increase of *orange zones*.

Based on the plots analysis, the number of required harmonics changes following a similar pattern when the amplitude is swept. With five or six harmonics, most of the range can be accessed, but higher harmonics are needed to

Parameter	Value
K	13.406 N/m
K_3	$3.768 \cdot 10^{10}\ N/m^3$
M	$5.6 \cdot 10^{-7}$ Kg
g_0	$5 \cdot 10^{-6}$ m
A_c	$3.86 \cdot 10^{-7}\ m^2$
ε	$8.85 \cdot 10^{-10}$
C_0	$6.83 \cdot 10^{-13}$ F
ω_n	4892 rad/s
f_n	0.78 kHz
$\beta - factor = K/(K_3\, g_0^2)$	14.23

Table 2: MEMS resonator parameters of the fabricated design in Fig. 1, used for the simulations.

reach larger amplitudes.

4.3.1 Voltage generation limitations

HBV patterns are complex depending on the desired oscillation parameters. Classical single harmonic driving voltages cannot generate those HBV patterns. That means that single harmonic driving schemes are limited on the selection of the desired output. Moreover, due to the nature of the electrostatic field generated in the parallel-plate capacitor, β_i terms are obtained by squaring the applied voltage. This condition adds more limitations to the achievable patterns in the driving force.

To understand the limitations in the generation of the driving voltage, a general case is analyzed including a large number of harmonics. If five harmonics are assumed in the driving voltage, it would be

$$\begin{aligned} V(t) = {} & \breve{V}_0 + \breve{V}_1 e^{j\omega t} + \breve{V}_{-1} e^{-j\omega t} + \breve{V}_2 e^{2j\omega t} + \breve{V}_{-2} e^{-2j\omega t} \\ & + \breve{V}_3 e^{3j\omega t} + \breve{V}_{-3} e^{-3j\omega t} + \breve{V}_4 e^{4j\omega t} + \breve{V}_{-4} e^{-4j\omega t} \\ & + \breve{V}_5 e^{5j\omega t} + \breve{V}_{-5} e^{-5j\omega t}, \end{aligned} \tag{25}$$

where $\breve{V}_0 = V_0$, $\breve{V}_i = -j\frac{V_i}{2} e^{j\phi_i}$ and $\breve{V}_{-i} = j\frac{V_i}{2} e^{-j\phi_i}$, being V_i the applied voltage for each harmonic.

Using these parameters definitions and equation (21), the β-terms are calculated as follows

$$
\begin{aligned}
\beta_0 &= V_0^2 + \frac{V_1^2}{2} + \frac{V_2^2}{2} + \frac{V_3^2}{2} + \frac{V_4^2}{2} + \frac{V_5^2}{2} \\
\beta_1 &= -jV_0V_1e^{j\phi_1} + \frac{V_1V_2}{2}e^{j(\phi_2-\phi_1)} + \frac{V_2V_3}{2}e^{j(\phi_3-\phi_2)} \\
&\quad + \frac{V_3V_4}{2}e^{j(\phi_4-\phi_3)} + \frac{V_4V_5}{2}e^{j(\phi_5-\phi_4)} \\
\beta_2 &= -\frac{V_1^2}{4}\,e^{2j\phi_1} - jV_0V_2\,e^{j\phi_2} + \frac{V_1V_3}{2}\,e^{j(\phi_3-\phi_1)} \\
&\quad + \frac{V_2V_4}{2}\,e^{j(\phi_4-\phi_2)} + \frac{V_3V_5}{2}\,e^{j(\phi_5-\phi_3)} \\
\beta_3 &= -\frac{V_1V_2}{2}\,e^{j(\phi_2+\phi_1)} - jV_0V_3\,e^{j\phi_3} + \frac{V_1V_4}{2}\,e^{j(\phi_4-\phi_1)} \\
&\quad + \frac{V_2V_5}{2}\,e^{j(\phi_5-\phi_2)} \\
\beta_4 &= -\frac{V_2^2}{4}\,e^{2j\phi_2} - \frac{V_1V_3}{2}\,e^{j(\phi_3+\phi_1)} - jV_0V_4\,e^{j\phi_4} \\
&\quad + \frac{V_1V_5}{2}\,e^{j(\phi_5-\phi_1)} \\
\beta_5 &= -\frac{V_2V_3}{2}\,e^{j(\phi_3+\phi_2)} - \frac{V_1V_4}{2}e^{j(\phi_4+\phi_1)} - jV_0V_5\,e^{j\phi_5} \\
\beta_6 &= -\frac{V_3^2}{4}\,e^{2j\phi_3} - \frac{V_2V_4}{2}\,e^{j(\phi_4+\phi_2)} - \frac{V_1V_5}{2}\,e^{j(\phi_5+\phi_1)} \\
\beta_7 &= -\frac{V_2V_5}{2}\,e^{j(\phi_5+\phi_2)} - \frac{V_3V_4}{2}\,e^{j(\phi_4+\phi_3)} \\
\beta_8 &= -\frac{V_4^2}{4}\,e^{2j\phi_4} - \frac{V_3V_5}{2}\,e^{j(\phi_5+\phi_3)} \\
\beta_9 &= -\frac{V_4V_5}{2}\,e^{j(\phi_5+\phi_4)} \\
\beta_{10} &= -\frac{V_5^2}{4}\,e^{2j\phi_5} \\
\beta_i &= 0 \;\text{ for } i \geq 11 \quad \textit{and} \quad \beta_{-i} = \overline{\beta_i} \;\text{ for } i.
\end{aligned}
$$

Analyzing the equations, an important conclusion is reached. Using only the first harmonic frequency in the input voltage, V_1, one can generate up to the β_2 term. If the input voltage has a second harmonic term, V_2, one can generate up to the β_4 term. And if the input voltage has up to the fifth harmonic term, V_5, one can generate up to the β_{10} term. This relationship can be extended to any input harmonic frequency term.

The number of β_i terms that can be produced squaring the input voltage can be compared with the previously derived number of harmonics needed from the HBV calculation, in Table 1. Table 3 shows that only the sets of equations of the Linear and Non-linear harmonic balance approximations with two harmonics in the output are completely well-defined with a voltage control. In these cases, it is possible to produce the needed β_i, for the whole set of equations. In the linear case, up to the third harmonic is needed in the input voltage, V_3, and in the nonlinear case, up to the fifth harmonic is needed in the input voltage, V_5.

In the rest of the cases, the mathematical equations are unbalanced, meaning that it is not possible to perfectly generate the right β_i for the needed oscillation and model. At this point, it is important to notice that a perfect sinusoidal oscillation is not mathematically possible with the available voltage actuation. On real world, almost perfect sinusoidal oscillation is possible because in the second harmonic oscillation case, which is well-defined, the amplitude of oscillation of the second harmonic can be chosen extremely small ($G_2 \simeq 0$), what leads to almost pure sinusoidal actuation. And this implies that the V_i-terms of the actuation voltage cancel out to leave only significant β_0 to β_5 terms for the nonlinear spring case.

Case	HBV Terms	Voltage terms
Linear spring 1 harmonic	β_0 to β_3	don't match
Linear spring 2 harmonics	β_0 to β_6	V_0, V_1, V_2, V_3
Linear spring 3 harmonics	β_0 to β_9	don't match
Nonlinear spring 1 harmonic	β_0 to β_5	don't match
Nonlinear spring 2 harmonics	β_0 to β_{10}	$V_0, V_1, V_2, V_3, V_4, V_5$
Nonlinear spring 3 harmonics	β_0 to β_{15}	don't match

Table 3: Comparison of the number of harmonic components needed in the HBV calculation, based on Table 1, and the terms that can be obtained by squaring the input voltage with one-sided actuation.

5 Minimum energy consumption

With HBV, the focus has been moved from choosing a voltage to selecting an oscillation amplitude and frequency. The next step is to find the minimum energy frequency for the selected amplitude. This frequency is equivalent to the resonance frequency in the linear case. However, in the nonlinear case, this minimum energy frequency depends on the selected amplitude and static bias.

The voltage magnitudes of the HBV give an indication of the maximum electrical load that must be applied, but they provide no insight on the energy consumption needed to sustain oscillation. Moreover, the needed voltage pattern can be really complex, and in those cases, the voltage magnitudes only capture the range of fluctuation of the signal but not its complexity.

The goal is to obtain the cheapest oscillation in energy consumption terms. In order to evaluate the HBV energy consumption, the actual voltage driv-

ing scheme including the voltage source must be analyzed (Fig. 8). In this set-up, the voltage source charges and discharges the driving capacitor (electrostatic transducer) with a series inductor and resistance, which is coupled to a mechanical load that moves due to the force generated by the electrostatic transducer [29].

The energy fed into the system by the voltage source is transformed into electrostatic potential energy by the capacitor, and this energy is converted into kinetic energy and mechanical potential energy during the oscillation. A MEMS resonator excited at resonance by an ideal voltage source would oscillate by itself if no mechanical dissipation would exist. However, this is not true in most cases. In real applications, the voltage source is not ideal, it compensates the damping losses and forces the oscillation at the driving frequency. Consequently, continuous energy supply exists, and the goal is to minimize it.

Introducing the voltage source as an active part in the circuit, as indicated in Fig. 8, the complete energy equation is as follows:

$$E(t) = \frac{1}{2}\mathrm{M}\dot{\hat{y}}(t)^2 + \frac{1}{2}\mathrm{K}\hat{y}(t)^2 + \frac{1}{4}\mathrm{K}_3\hat{y}(t)^4 + \frac{1}{2C(t)}q(t)^2 + \frac{1}{2}\mathrm{L}_{vs}\dot{q}^2 \quad (26)$$

where $q(t)$ is the charge accumulated in the capacitor, the capacitor capacitance is, as expected, $C(t) = \frac{\mathrm{C}_0}{(1-\frac{\hat{y}(t)}{\mathrm{g}_0})}$ and L_{sv} is the voltage source inductance, if present.

The interest is on how the energy is exchanged in the system, what implies studying the energy variation

$$\frac{d}{dt}E(t) = \mathrm{M}\ddot{\hat{y}}(t)\dot{\hat{y}}(t) + \mathrm{K}\hat{y}(t)\dot{\hat{y}}(t) + \mathrm{K}_3\hat{y}(t)^3\dot{\hat{y}}(t) - \frac{1}{2C(t)^2}\frac{\partial C(t)}{\partial \hat{y}(t)}\dot{\hat{y}}(t)q(t)^2 + \frac{1}{C(t)}q(t)\dot{q}(t) + \mathrm{L}_{vs}\dot{q}(t)\ddot{q}(t)$$

where $\dot{q}(t)$ is the time derivative of the charge.

Using the dynamic equations of the coupled system (Fig. 8), obtained via Lagrange formulation

$$\mathrm{M}\ddot{\hat{y}}(t) + \mathrm{B}\dot{\hat{y}}(t) + \mathrm{K}\hat{y}(t) + \mathrm{K}_3\hat{y}(t)^3 = \frac{\frac{\partial C(t)}{\partial \hat{y}(t)}}{2C(t)^2}q(t)^2 \quad (27)$$

$$\mathrm{L}_{vs}\ddot{q}(t) + \frac{1}{C(t)q(t)} + \mathrm{R}_{vs}\dot{q}(t) = V_{vs}(t) \quad (28)$$

and rearranging the terms in the energy variation equation

$$\frac{d}{dt}E(t) = \left(\mathrm{M}\ddot{\hat{y}}(t) + \mathrm{K}\hat{y}(t) + \mathrm{K}_3\hat{y}(t)^3 - \frac{1}{2C(t)^2}\frac{\partial C(t)}{\partial \hat{y}(t)}q(t)^2\right)\dot{\hat{y}}(t) + \dot{q}(t)\left(\frac{1}{C(t)}q(t) + \mathrm{L}_{vs}\ddot{q}(t)\right),$$

the energy variation reduces to

$$\frac{d}{dt}E(t) = -\mathrm{B}\dot{\hat{y}}(t)^2 - \mathrm{R}_{vs}\dot{q}(t)^2 + \dot{q}(t)V_{vs}(t). \tag{29}$$

And substituting the charge by the voltage and current equivalence

$$q(t) = C(t)\,V(t)\,,\ \dot{q} = I_{vs}(t)$$

the final formulation is obtained

$$\frac{d}{dt}E(t) = -\mathrm{B}\dot{\hat{y}}(t)^2 - \mathrm{R}_{vs}I_{vs}(t)^2 + V_{vs}(t)I_{vs}(t). \tag{30}$$

The energy variation has a part that corresponds to the energy mechanically dissipated in the damper (B), a part that is electrically dissipated in the voltage source and system resistance (R_{vs}) and another part that corresponds to the power supplied by the voltage source ($V_{vs}(t)I_{vs}(t)$).

Assuming steady-state oscillation, the energy balance in one oscillation cycle ($T_c = \frac{2\pi}{\omega}$) must be zero, then from equation (30), we obtain

$$\begin{aligned}\frac{1}{T_c}\int_0^{T_c}\frac{d}{dt}E(t)dt = 0 = -\frac{1}{T_c}\int_0^{T_c}\mathrm{B}\dot{\hat{y}}(t)^2dt \\ -\frac{1}{T_c}\int_0^{T_c}\mathrm{R}_{vs}I_{vs}(t)^2dt + \frac{1}{T_c}\int_0^{T_c}V_{vs}(t)I_{vs}(t)dt\end{aligned} \tag{31}$$

and from this equation, the energy provided by the voltage source can be isolated as

$$\begin{aligned}\frac{1}{T_c}\int_0^{T_c}V_{vs}(t)I_{vs}(t)dt = \\ \frac{1}{T_c}\int_0^{T_c}\mathrm{B}\dot{\hat{y}}(t)^2dt + \frac{1}{T_c}\int_0^{T_c}\mathrm{R}_{vs}I_{vs}(t)^2dt\end{aligned} \tag{32}$$

meaning that the voltage source is used to compensate, as expected, two energy losses: the damping of the system and the source/circuitry losses. If we could assume that the source is ideal, all the losses would be due to the damping of the MEMS resonator. And if the MEMS resonator could have no damping, then, the voltage source would have zero energy balance, as the current delivered during the charging of the capacitor would be returned during discharging.

However, in real applications the losses exist, and as the goal is to optimize the energy consumption for sinusoidal oscillation, the actual energy losses in an oscillation cycle must be calculated. If the oscillation is fixed to be a perfect sinusoidal

$$\hat{y}(t) = \hat{Y}_0 + \hat{Y}_1\sin(\omega t) \tag{33}$$

$$\dot{\hat{y}}(t) = \hat{Y}_1\omega\cos(\omega t), \tag{34}$$

the electrical energy consumed by the voltage source is given by (32), where the mechanical part can be solved leaving

$$E_{losses} = \frac{1}{T_c}\int_0^{T_c} V_{vs}(t) I_{vs}(t) dt = \frac{\mathrm{M}\omega_\mathrm{n}}{2\mathrm{Q}}\,\hat{Y}_1^2\,\omega^2 + \frac{1}{T_c}\int_0^{T_c} \mathrm{R}_{vs} I_{vs}(t)^2 dt. \quad (35)$$

Consequently, the energy consumed has two terms. The first term is proportional to the square of the oscillation frequency, proportional to the square of the amplitude of oscillation and inversely proportional to the Quality factor. And the other one is dependant on the dissipated power in the voltage source resistor and circuitry.

As HBV is known, and consequently $I_{vs} = \frac{d(C(t)V(t))}{dt}$, the estimated energy consumption for each driving scheme can be calculated and compared.

Fig. 9 shows that the damping losses vary a lot due to the Quality factor and the amplitude of oscillation. Once those parameters are chosen, the energy variation is not large, for the usual range of frequencies. In the example, the range of frequencies varies from $0.8\omega_\mathrm{n}$ to $1.2\omega_\mathrm{n}$, the Quality-factor ranges from 10 to 1000000 and the amplitude of oscillation is fixed at $0.4\mathrm{g}_0$ and $0.7\mathrm{g}_0$. As expected, the damping losses are lower at low amplitudes and low frequencies.

In comparison, the electrical losses are only slightly affected by the Quality factor, and have a strong dependency on the frequency and amplitude of oscillation. Fig. 10a shows the electrical losses for an amplitude of $0.7\mathrm{g}_0$, a static bias of $0.95\mathrm{g}_0$ and a Quality factor ranging from 100 to 1000000. In the plot, the three energy curves are almost overlapped. As can be observed, the electrical losses define a low-energy frequency, that is associated to the resonant-like behavior of the nonlinear system.

Fig. 10b compares the electrical and mechanical losses in an example. The total resistance is assumed to be 1 $k\Omega$. As can be seen, for this value, damping losses are similar to electrical losses in high-vacuum conditions ($\mathrm{Q} = 1000000$). Combination of both energy losses defines a low energy frequency, that is not exactly the same that can be obtained from the electrical losses.

Fig. 11a shows the steady-state electrical energy consumption calculation for amplitudes from $0.3\mathrm{g}_0$ to $0.8\mathrm{g}_0$, for an oscillation with a Quality factor of 100 and static bias of $0.95\mathrm{g}_0$. As amplitude increases, energy consumption increases, as expected. But at the same time, the frequency range with one-sided actuation decreases and the minimum oscillation frequency shifts to natural frequency and far beyond. This leads to an unexpected conclusion. In some cases, frequencies higher than natural frequency can lead to more energy efficient system driving.

Fig. 11b shows the same system, but this time the oscillation amplitude is fixed to $0.4\mathrm{g}_0$, the Quality factor is 100 and the static gap bias is ranged from 0.9 to 0.99. The energy plots show that, for each bias, a different minimum energy frequency exists again. The variation of the gap bias don't produce large frequency variations as in the previous case. There is a limitation, the

curves show that as the bias is close to the unit (no bias), the range of feasible frequencies gets reduced, due to the use of one-sided voltage actuation.

As a conclusion, Harmonic Balance allows to choose the minimum energy consumption frequency of oscillation depending on the desired oscillation. And as can be seen in the plots, the difference in energy consumption can be relevant. Moreover, Harmonic Balance energy analysis is critical. Depending on the desired oscillation amplitude, results can lead to unexpected range of energy-efficient frequencies.

6 Full range oscillation selection

6.1 One-sided actuation limitations

In the literature, most strategies are based on one-sided actuation. Even when the designed devices have driving electrodes in both sides [2]. This occurs when the same driving voltage (phase-shifted) is used on both sides, just to increase the driving force [27].

The HBV shows that the range of oscillations that can be achieved is limited using this actuation scheme (*Red zone* in Fig. 7). Moreover, it forces to have large static displacements in order to increase the amplitude of the oscillation.

The need of two-sided actuation had already been presented in [27], as a way to guarantee no static displacement. HBV analysis extends that result and highlights the limitations introduced by one-sided actuation in order to select the frequency, static displacement and amplitude of oscillation.

Consequently, to be able to use the full capability of the HBV, two-sided actuation must be implemented.

6.2 Harmonic Balance Voltage two-sided actuation

A new two-sided actuation approach is presented to overcome the limitation of one-sided actuation, and being able to use HBV to freely choose the oscillation in the whole feasible range. The approach is based on understanding the force that must be generated by the V^2 action, instead of trying to generate the needed voltage. If the device, instead of being actuated just by one side as Fig. 12, is actuated by two opposite sides, Fig. 13, the total force can be reproduced in all cases, even when $V_{\mathrm{HBV}}(t)^2$ is negative-valued. Consequently, it is needed to have a two-sided actuator in the MEMS device to overcome the problem, splitting the needed voltage between the actuators and generating the desired driving force into the MEMS resonator.

The desired actuation force has the following form:

$$F = \frac{\mathrm{f}_k \mathrm{g}_k}{g^2} V^2. \tag{36}$$

Assume that V^2 driving voltage can be divided in V_+^2, its positive part, and

V_-^2, its absolute value negative part, giving place to

$$V^2 = V_+^2 - V_-^2.$$

Assume that V_{d1} is applied to one side of the MEMS resonator and V_{d2} to the other side. And that the normalized gap in each actuator is $g_1 = g$ and $g_2 = 2 - g$. Then, the desired force is divided between actuators in the following way:

$$\frac{\mathrm{f}_k \mathrm{g}_k}{g^2} V^2 = \frac{\mathrm{f}_k \mathrm{g}_k}{g_1^2} V_{d1}^2 - \frac{\mathrm{f}_k \mathrm{g}_k}{g_2^2} V_{d2}^2. \tag{37}$$

The negative signs appears because forces are in opposed directions.

The key is then to select the right values for V_{d1} and V_{d2} actuation voltages. The following equations allow to calculate those values

$$V_{d1} = \sqrt{V_+^2} \tag{38}$$

$$V_{d2} = \frac{g_2 \sqrt{V_-^2}}{g_1} = \frac{(2-g)\sqrt{V_-^2}}{g} \tag{39}$$

and they generate the desired force over the MEMS resonator with two-sided actuation

$$\begin{aligned} \frac{\mathrm{f}_k \mathrm{g}_k}{g^2} V^2 &= \frac{\mathrm{f}_k \mathrm{g}_k}{g^2} \sqrt{V_+^2}^2 - \frac{\mathrm{f}_k \mathrm{g}_k}{(2-g)^2} \left(\frac{(2-g)\sqrt{V_-^2}}{g} \right)^2 \\ &= \frac{\mathrm{f}_k \mathrm{g}_k}{g^2} V_+^2 - \frac{\mathrm{f}_k \mathrm{g}_k}{g^2} V_-^2 \\ &= \frac{\mathrm{f}_k \mathrm{g}_k}{g^2} (V_+^2 - V_-^2). \end{aligned} \tag{40}$$

This approach has been successfully tested in the simulations, as can be shown in Fig. 14.

The new drive approach overcomes the limitations of the one-sided actuation. HBV two-sided actuation with separated voltage action to each electrode allows to oscillate any MEMS resonator at any desired amplitude and bias, within physical constrains.

As shown in Fig. 15, in terms of electrical energy consumption the two-sided actuation is always more energy demanding. But as has been seen in the energy analysis, the combination of electrical losses and damping losses can lead to working points where two-sided actuation can be interesting. Moreover, the range of feasible frequencies with one-sided actuation becomes very narrow (Fig. 11) for some desired amplitudes of oscillation. And other amplitudes are not even achievable, what leads to the necessity of two-sided actuation.

The use of HBV two-sided actuation allows smooth operation of the resonator in a large range of amplitudes and frequencies. This opens a new area of research to develop new control algorithms for the stable oscillation of the MEMS resonators.

The main drawback of two-sided actuation is that real-time position feedback is needed in order to generate the appropriate actuation voltage. However, this can be overcome with known techniques as Electromechanical Amplitude Modulation (EAM) [30].

7 Conclusions

The typical use of a sinusoidal driving voltage signal with only the first harmonic always generates outputs with first and second harmonic components, due to the nonlinear nature of the parallel-plate electrostatic actuator. The existence of the V^2 term leads to a nonlinear response, with the possibility of non-pure-sinusoidal responses. Moreover, the desired static bias and oscillation amplitude cannot be chosen, as they are fixed by the magnitude of the input voltage.

A perfect sinusoidal output can only be achieved with an input signal with the appropriate form and number of harmonics. As desired amplitude increases, the number of needed harmonics also increases. Although a closed-form analytical solution has not been obtained, the combination of HBV calculations and the use of numerical solution allows to choose the right input signal to reach the desired oscillation in most of the available oscillation range. Examples show the viability under changes of damping and frequency of oscillation.

The use of Harmonic Balance Voltage to choose the desired oscillation amplitude and frequency breaks the usual concept of resonant frequency associated with a fixed sinusoidal driving with a DC load plus and AC load. Now, any combination of oscillation amplitude and frequency is possible. And for each amplitude of oscillation a minimum energy frequency can be selected. The only constrain is the ability to apply the calculated voltage. Some voltages cannot be generated with one-sided actuation, but this can be achieved using the introduced HBV two-sided configuration.

Consequently, the introduction of the Harmonic Balance Voltage leads to a new paradigm on how actuating parallel-plate electrostatically actuated MEMS resonators.

Two concerns raise from the Harmonic Balance Voltage approach, and must be addressed in future research. Harmonic Balance Voltage is based on steady-state oscillation, so transient evolution to reach the desired oscillation must be appropriately selected to avoid AC pull-in. And HBV should be readily calculated in order to be applied on a real device.

These concerns lead to the necessity of proposing a new control strategy where the controller should be able to produce the desired frequency components for the driving voltage, adapt them to the desired amplitude and bias, and ensure the stability of the oscillation at minimum energy consumption. All these, while it should avoid AC pull-in.

References

[1] Abdel-Rahman, E.M., Nayfeh, A.H., Younis, M.I.: Dynamics of an electrically actuated resonant microsensor. In: Proceedings of the International Conference on MEMS, NANO and Smart Systems, pp. 188–196 (2003)

[2] Acar, C., Shkel, A.M.: Inherently robust micromachined gyroscopes with 2-DOF sense-mode oscillator. IEEE/ASME Journal of Microelectromechanical Systems **15**, 380–387 (2006)

[3] Alsaleem, F.M., Younis, M.I., Ruzziconi, L.: An experimental and theoretical investigation of dynamic pull-in in mems resonators actuated electrostatically. IEEE/ASME Journal of Microelectromechanical Systems **19**(4) (2010)

[4] Bouchaala, A., Jaber, N., Yassine, O., Shekhah, O., Chernikova, V., Eddaoudi, M., Younis, M.I.: Nonlinear-based mems sensors and active switches for gas detection. Sensors **16**(6), 758 (2016)

[5] Busta, H., Amantea, R., Furst, D., Chen, J.M., Turowski, M., Mueller, C.: A MEMS shield structure for controlling pull-in forces and obtaining increased pull-in voltages. Journal of Micromechanics and Microengineering **11**(6), 720–725 (2001)

[6] Chu, P., Pister, S.: Analysis of closed-loop control of parallel-plate electrostatic microgrippers. In: Proceedings of the IEEE International Conference on Robotics and Automation, vol. 1, pp. 820–825 (1994)

[7] Daqaq, M., Reddy, C., Nayfeh, A.: Input-shaping control of nonlinear mems. Nonlinear Dynamics **54**(1-2), 167–179 (2008)

[8] Fargas-Marquès, A., Casals-Terre, J., Shkel, A.M.: Resonant pull-in condition in parallel-plate electrostatic actuators. IEEE/ASME Journal of Microelectromechanical Systems **16**(5), 2006-0147 (2007)

[9] Gallacher, B.J., Burdess, J.S., Harish, K.M.: A control scheme for a mems electrostatic resonant gyroscope excited using combined parametric excitation and harmonic forcing. Journal of Micromechanics and Microengineering **16**(2), 320–331 (2006)

[10] Hsu, W.T., Clark, J.R., Nguyen, C.T.C.: A Resonant Temperature Sensor Based on Electrical Spring Softening, pp. 1456–1459. Springer Berlin Heidelberg (2001)

[11] Huang, J., Liew, K., Wong, C., Rajendran, S., Tan, M., Liu, A.Q.: Mechanical design and optimization of capacitive micromachined switch. Sensors and Actuators A: Physical **93**, 273–285 (2001)

[12] Hung, E.S., Senturia, S.D.: Extending the travel range of analog-tuned electrostatic actuators. IEEE/ASME Journal of Microelectromechanical Systems **8**, 497–505 (1999)

[13] Ilyas, S., Ramini, A., Arevalo, A., Younis, M.I.: An experimental and theoretical investigation of a micromirror under mixed-frequency excitation. Journal of Microelectromechanical Systems **24**(4), 1124–1131 (2015)

[14] Jaber, N., Ramini, A., Carreno, A.A.A., Younis, M.I.: Higher order modes excitation of electrostatically actuated clampedclamped microbeams: experimental and analytical investigation. Journal of Micromechanics and Microengineering **26**(2), 025,008 (2016)

[15] Jaber, N., Ramini, A., Hennawi, Q., Younis, M.: Wideband MEMS resonator using multifrequency excitation. Sensors and Actuators A: Physical **242**, 140 – 145 (2016)

[16] Jaber, N., Ramini, A., Younis, M.I.: Multifrequency excitation of a clamped-clamped microbeam: Analytical and experimental investigation. Microsystems & Nanoengineering **2**, 16,002 (2016)

[17] Krylov, S., Bernstein, Y.: Large displacement parallel plate electrostatic actuator with saturation type characteristic. Sensors and Actuators A: Physical **130-131**, 497–512 (2006)

[18] Kudrle, T., Shedd, G., Wang, C., Hsiao, J., Bancu, M., Kirkos, G., Yazdi, N., Waelti, M., Sane, H., Mastrangelo, C.: Pull-in suppression and torque magnification in parallel plate electrostatic actuators with side electrodes. In: Proceedings of the International Conference on Solid State Sensors and Actuators, TRANSDUCERS (2003)

[19] Nguyen, Q.C., Krylov, S.: Nonlinear tracking control of vibration amplitude for a parametrically excited microcantilever beam. Journal of Sound and Vibration **338**, 91 – 104 (2015)

[20] Ouakad, H.M., Younis, M.I.: Dynamic response of mems sensor near fundamental and higher-order frequencies. In: IEEE SENSORS 2014 Proceedings, pp. 1956–1959 (2014)

[21] Painter, C.C., Shkel, A.M.: Active structural error suppression in MEMS vibratory rate integrating gyroscopes. IEEE Sensors Journal **3**(5), 595–606 (2003)

[22] Rhoads, J.F., Shaw, S.W., Turner, K.L.: The nonlinear response of resonant microbeam systems with purely-parametric electrostatic actuation. Journal of Micromechanics and Microengineering **16**(5), 890–899 (2006)

[23] Rocha, L.A., Cretu, E., Wolffenbuttel, R.F.: Using dynamic voltage drive in a parallel-plate electrostatic actuator for full-gap travel range and positioning. IEEE/ASME Journal of Microelectromechanical Systems **15**(1), 69–83 (2006)

[24] Roessig, T.W.: Integrated MEMS tuning fork oscillators for sensor applications. Ph.D. thesis, U.C. Berkeley (1998)

[25] Rosa, M.A., Bruyker, D.D., Vlkel, A.R., Peeters, E., Dunec, J.: A novel external electrode configuration for the electrostatic actuation of mems based devices. Journal of Micromechanics and Microengineering **14**, 446–451 (2004)

[26] Seeger, J., Crary, S.: Stabilization of electrostatically actuated mechanical devices. In: Proceedings of the International Conference on Solid State Sensors and Actuators, TRANSDUCERS, vol. 2, pp. 1133–1136 (1997)

[27] Seeger, J.I., Boser, B.E.: Parallel-plate driven oscillations and resonant pull-in. In: Solid-State Sensor, Actuator and Microsystems Workshop, Hilton Head Island, pp. 313–316 (2002)

[28] Seleim, A., Towfighian, S., Delande, E., Abdel-Rahman, E., Heppler, G.: Dynamics of a close-loop controlled mems resonator. Nonlinear Dynamics **69**(1), 615–633 (2012)

[29] Senturia, S.: Microsystem Design, 1st edn. Kluwer Academic Publishers (2001)

[30] Trusov, A., Shkel, A.: A novel capacitive detection scheme with inherent self-calibration. IEEE/ASME Journal of Microelectromechanical Systems **16**(6), 1324–1333 (2007). DOI 10.1109/JMEMS.2007.906077

[31] Wu, J., Carley, L.: Electromechanical $\Delta\Sigma$ modulation with high-q micromechanical accelerometers and pulse density modulated force feedback. IEEE Transactions on Circuits and Systems I: Regular Papers **53**(2), 274–287 (2006)

[32] Younis, M., Abdel-Rahman, E., Nayfeh, A.H.: A reduced-order model for electrically actuated microbeam-based MEMS. IEEE/ASME Journal of Microelectromechanical Systems **12**, 672–680 (2003)

[33] Younis, M.I.: Multi-mode excitation of a clamped–clamped microbeam resonator. Nonlinear Dynamics **80**(3), 1531–1541 (2015)

a)

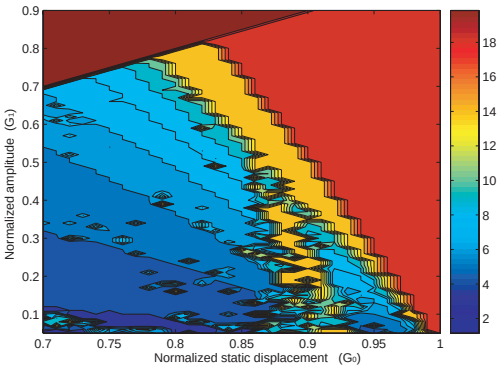

b)

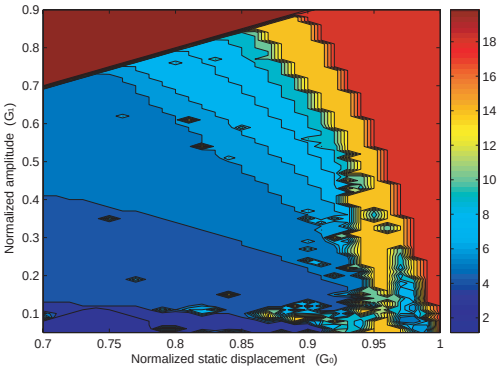

c)

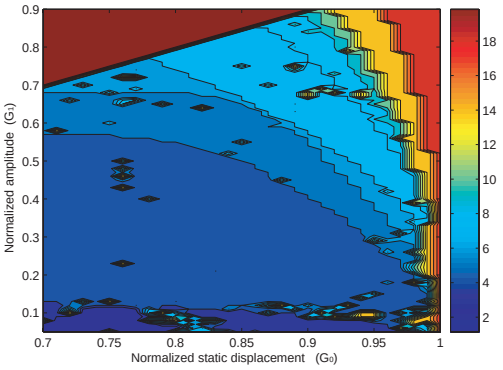

Figure 7: Number of harmonics needed to reproduce HBV using a nonlinear spring model. Selected damping is Q = 100 and different frequencies are tested: a) $0.9\omega_{\mathrm{n}}$ b) $0.96\omega_{\mathrm{n}}$ c) ω_{n}.

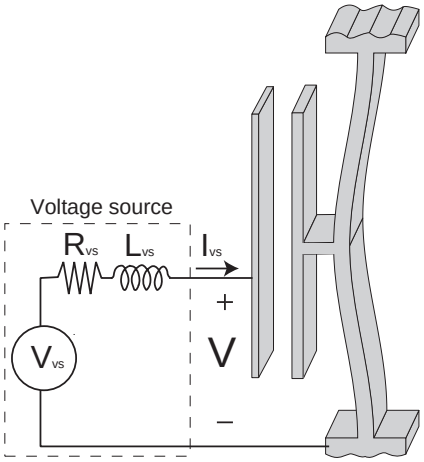

Figure 8: Electrical coupling of the electromechanical system including the voltage source, based on [29].

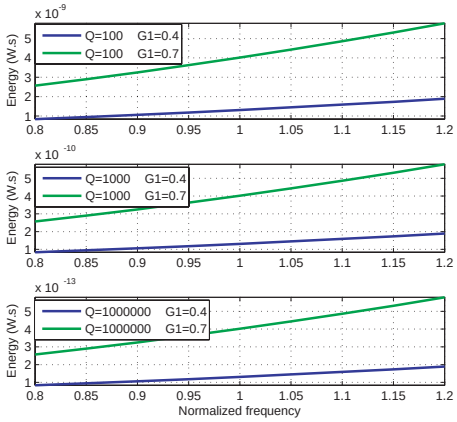

Figure 9: Energy losses due to mechanical system damping for three different Quality-factors and two different oscillation amplitudes, for the MEMS resonator values in Table 2.

a)

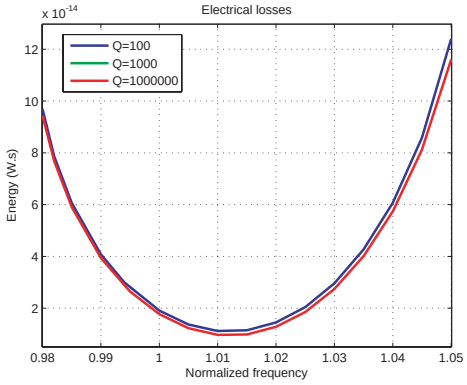

b)

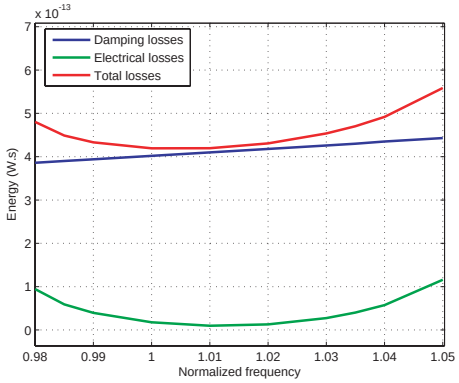

Figure 10: a) Electrical energy losses for three different Quality-factors, an oscillation amplitude of $0.7g_0$ and a static bias of $0.95g_0$, for the MEMS resonator values in Table 2. Curves for Q = 1000 and Q = 1000000 are overlapped. b) Comparison of the magnitude of the electrical losses and the damping losses. System analyzed for an oscillation amplitude of $0.7g_0$, a static bias of $0.95g_0$ and a high-vacuum Quality factor (Q = 1000000).

a)

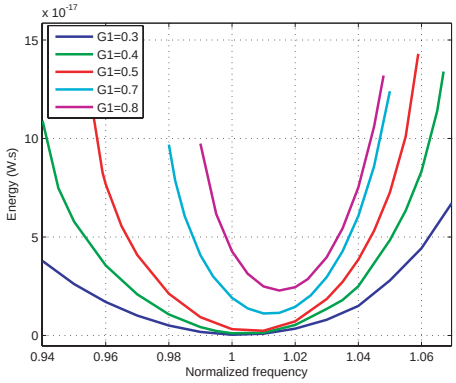

b)

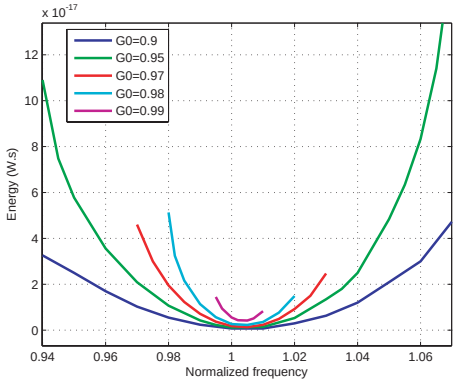

Figure 11: Steady-state electrical energy consumption curves based on the calculated HBV for fixed damping at Q = 100. a) The static bias is fixed at $0.95g_0$, and the desired amplitude of oscillation ranges from $0.3g_0$ to $0.8g_0$. b) The desired amplitude of oscillation is fixed at $0.4g_0$ and the static bias is varied between $0.9g_0$ and $0.99g_0$.

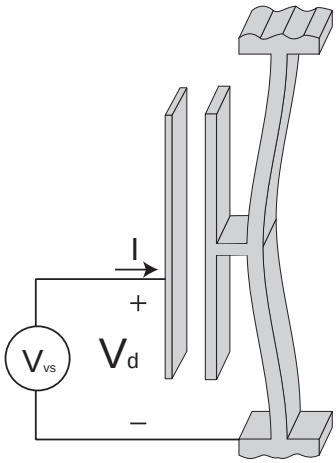

Figure 12: Schematic MEMS resonator with one driving port (V_d).

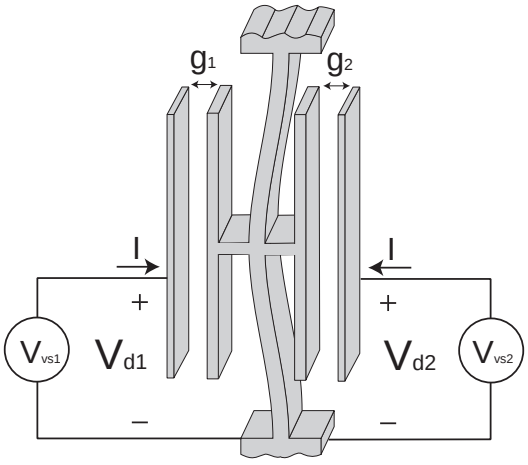

Figure 13: Schematic MEMS resonator with two driving ports (V_{d1} and V_{d2}).

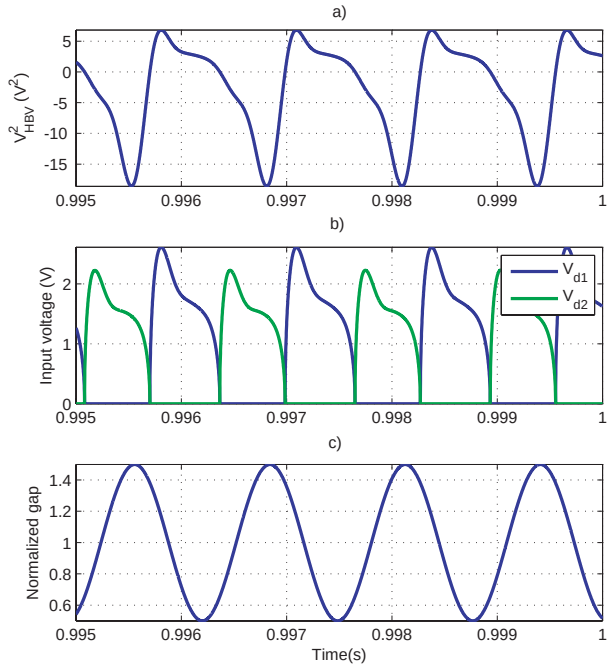

Figure 14: HBV generation to oscillate the system with a damping of Q = 100, at natural frequency, with a static gap position of $G_0 = 1$ and an amplitude of oscillation of $G_1 = 0.5$. a) $V_{\mathrm{HBV}}(t)^2$ b) HBV two-sided voltages V_{d1} and V_{d2}. c) Resulting simulated gap oscillation with the desired pattern.

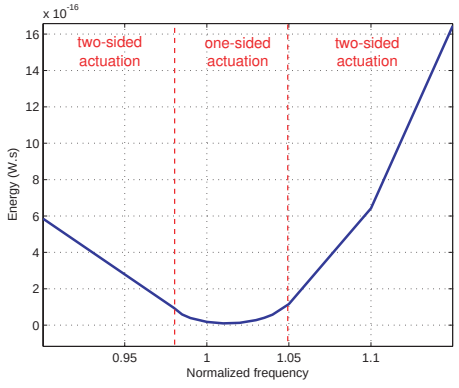

Figure 15: Energy consumption curve adding two-sided range to the HBV one-sided energy calculation of previous section, for fixed damping at Q = 100. Amplitude of desired oscillation $0.7\mathrm{g}_0$ with 0.95 gap bias.